




Role of cluster configurations in the elastic scattering of light projectiles on ^{58}Ni and ^{64}Zn targets: a phenomenological analysis

A tribute to Mahir S. Hussein

V. Guimarães^{1,a} , E. N. Cardozo², J. Lubian², M. Assunção³, K. C. C. Pires¹, L. F. Canto⁴, B. Mukeru⁵, G. Kaur¹, E. F. Aguilera⁶

¹ Instituto de Física, Universidade de São Paulo, Rua do Matão 1371, 05508-090 São Paulo, SP, Brazil

² Instituto de Física, Universidade Federal Fluminense, Avenida Litorânea s/n, Gragoatá, Niterói, RJ 24210-340, Brazil

³ Departamento de Física, Universidade Federal de São Paulo, CEP 09913-030, Diadema, SP, Brazil

⁴ Universidade Federal do Rio de Janeiro, CP 68528 Rio de Janeiro, RJ, Brazil

⁵ Department of Physics, University of South Africa, PO Box 392, Pretoria 0003, South Africa

⁶ Departamento de Aceleradores, Instituto Nacional de Investigaciones Nucleares, Apartado Postal 18-1027, Código Postal 11801, Mexico, DF, Mexico

Received: 23 November 2020 / Accepted: 19 February 2021 / Published online: 8 March 2021

© The Author(s), under exclusive licence to Società Italiana di Fisica and Springer-Verlag GmbH Germany, part of Springer Nature 2021
Communicated by Nicolas Alamanos

Abstract Motivated by the strong synergy between structure and nuclear reactions we have performed a phenomenological analysis using available elastic scattering data for collisions of tightly-bound (^{10}Be , ^{10}B , ^{10}C , ^{11}B , ^{12}C , ^{16}O), weakly-bound (^6Li , ^7Li , ^8Li , ^9Be), and exotic (^6He , ^8B and ^{11}Be) nuclei on ^{58}Ni and ^{64}Zn targets at energies close to the Coulomb barrier. After a proper reduction, the cluster configuration and dynamics effects in the total reaction cross section are discussed. Also, an approach based on the interaction distances is used to investigate static and dynamic effects in the elastic scattering of light nuclei. A correlation between the critical interaction distance and binding energy for a given configuration is observed.

1 Introduction

Elastic scattering is the simplest process which can occur in collisions of two nuclei. It involves few degrees of freedom and the cross sections at energies close to the Coulomb barrier are quite large. Over the years, several experiments on elastic scattering have been performed. Compilation of the several data set related to these experiments can be found, for instance, in the EXFOR database [1] and NRV project [2,3]. The results of the analysis of these experiments have improved our understanding on the interaction mechanism between heavy nuclei and their structures. Prof. Hussein had an important involvement in this endeavor and his strong

interest in the scattering and reaction theories led him to the development of the formal complex potential scattering theory [4,5]. Besides these two works, Hussein has an extensive number of other publications related to the development of the theory of elastic scattering [6–9]. In nowadays, elastic scattering experiments are still being used to probe the surface structure of nuclei. In particular, with the possibility of using radioactive ion projectiles, their static (cluster configuration and deformations) and dynamics (coupling channels) effects can be investigated [10]. The last contribution of Hussein in the field was a review paper recently published on the total reaction cross section [11] and a previous review in Ref. [12].

The investigation of the interplay between structure and nuclear reactions is still very alive due to the strong synergy between the configuration and dynamics of the process involved in reactions induced by exotic and weakly bound (stable and radioactive) nuclei. The weak binding energy of the valence or cluster particle for some of these nuclei makes them easy to break during the interaction with a target, favoring couplings to the continuum [13,14]. Microscopic theory, where the projectile is described by cluster model, has been developed by Descouvemont and Hussein [15]. This microscopic generalization (MCDCC) calculations relies only on nucleon-target interactions, and therefore the cluster configuration of the projectile plays a quite important role in describing the elastic scattering process.

The clustering phenomenon is important in nuclei such as $^6,^8\text{He}$, $^{6,7,8}\text{Li}$, $^{10,12}\text{Be}$ and $^{10,12,14}\text{C}$. Some very weakly-

^a e-mail: valdir.guimaraes@usp.br (corresponding author)

bound nuclei, such as ${}^6\text{He}$, ${}^8\text{B}$, ${}^{11}\text{Li}$ and ${}^{11}\text{Be}$ can also form unusual configurations and are called *exotic* nuclei. One of such unusual configuration occurs when a core nucleus is surrounded by one or more weakly-bound valence nucleons. If these valence particles are bound to the core in a predominant *s-wave* relative orbital, the matter distribution at the surface will form a so-called *halo* configuration, in which the loosely-bound valence nucleons are found at much greater distances from the core. Also, nuclei such as ${}^{11}\text{Li}$ and ${}^6\text{He}$ form a *borromean* system in which the corresponding inert core and two valence neutrons (*core* – *n* – *n*) are bound together in such a way that, if one of them is removed, the remaining two-body subsystems (*core* – *n* or *n* – *n*) becomes unbound and breaks apart. With similar characteristics, the proton-rich carbon isotope ${}^{10}\text{C}$ is also an interesting nucleus. This nucleus can be considered to have a 4-body configuration: $\alpha - \alpha - p - p$. After removing any one of these particles, the remaining nucleus also breaks apart. Due to this 4-body configuration, ${}^{10}\text{C}$ is the only nucleus supposed to have a *brunnian* (*super-borromean*) structure [16, 17], where the three interactions of the constituent particles can be associated with four interconnected rings. These *halo*, *borromean* and *brunnian* structures differ significantly from that of ordinary nuclei which have a well-defined surface. For a review of the halo structure of exotic nuclei, see for instance Ref. [18] and references therein. The exotic geometries of these nuclei (static effects) can strongly influence the dynamics of reactions induced by such systems. The nuclear radii of these systems therefore do not follow the conventional $R = r_0 \times A^{1/3}$, with $r_0 \approx 1.3$ fm, expression.

Due to its high cross section, when compared with other direct reactions, the elastic scattering process has been used to investigate the structure of light radioactive ion projectiles. The description of the cross sections for elastic scattering is very sensitive to the interaction potential between the projectile and target nuclei and to the structure of the nuclei involved. Thus, analysis of elastic scattering angular distributions measured at energies near the Coulomb barrier can provide valuable information on both the static and dynamics effects of weakly-bound nuclei. In particular, elastic scattering induced by exotic nuclei, at energies close to the Coulomb barrier, has shown interesting and intriguing coupling effects. For instance, the unusual cluster configurations of exotic nuclei can produce strong couplings to the continuum introducing characteristic dynamic polarization (attractive or repulsive) in the optical potential, which is not present in the elastic scattering induced by strongly-bound projectiles.

Although some advances have been achieved in the understanding of the nuclear interaction induced by weakly-bound and/or exotic nuclei, the influence of the breakup and dynamic effects is still not completely known. We have contributed to these issues by performing several experiments on

elastic scattering with ${}^6\text{He}$ [19], ${}^8\text{Li}$ [20], ${}^7\text{Be}$ and ${}^8\text{B}$ [21], ${}^{10}\text{B}$ [22], ${}^{11}\text{B}$ [23], ${}^{12}\text{B}$ [24, 25], and ${}^{10}\text{C}$ [26] nuclei as projectile on ${}^{58}\text{Ni}$ targets. All these elastic scattering data have been analyzed in terms of coupled-channel calculations, as reported in their specific papers. However, systematic analysis within the same framework, involving a combination of several data set, can be a powerful tool to investigate general behavior and, at the same time, emphasize particular properties. A systematic analysis on the static and dynamic features in the elastic scattering of the boron isotopes, ${}^8\text{B}$, ${}^{10}\text{B}$, ${}^{11}\text{B}$ and ${}^{12}\text{B}$ on ${}^{58}\text{Ni}$ target, was performed showing that the different cluster configuration of the boron isotopes lead to a different prevalent effect in elastic scattering [27]. For instance, the proton-rich nucleus ${}^8\text{B}$ has a very low proton binding energy, $S_p = 0.138$ MeV, for the ${}^7\text{Be} + p$ decay, while ${}^{11}\text{B}$ is quite tightly-bound with binding energy of $S_\alpha = 8.664$ MeV. The ${}^{10}\text{B}$ in its turn, is a well deformed nucleus, with the largest spin (3^+) among boron isotope chain, while ${}^{12}\text{B}$ nucleus is radioactive with a low deformation and low spin.

An alternative approach to investigate the influence of the direct reactions on the total reaction cross section is the comparison of different systems containing data for both tightly and weakly bound nuclei. However, since the cross sections are also influenced by trivial factors like geometry, energy, atomic and mass numbers of the collision partners, some reduction procedure is necessary before the comparison of the cross sections is performed. This reduction can be obtained by considering some expression to transform collision energies and the total reaction cross sections in a such way that the dependence of the reduced data on the system's masses and charges becomes very weak.

In the present work we performed a phenomenological systematic analysis based on the total reaction cross sections and interaction distances, using elastic data of light projectiles available in the literature on ${}^{58}\text{Ni}$ and ${}^{64}\text{Zn}$ targets. This paper is organized as follows. In Sect. 2 we introduced the reduction method used for the total reaction cross section, emphasizing the importance of direct reactions. In Sect. 3 we developed the analysis based on interaction distance normalized by the distance of closest approach, while in Sect. 4 we have the summary.

2 Total reaction cross section

The total reaction cross section, σ_R , is a very important quantity in collisions of heavy nuclei (see, e.g., Ref. [11]). It may contain information about the size, geometry, deformation, of the colliding partners as well as on the open channels in the collision. Measurements of the cross sections for the individual channels, that compose the total reaction cross section, although very desirable, is very difficult and it is still a challenge for experimentalists. It would require different setups

to measure the products from different reactions. This has been achieved for very few systems such as ${}^6\text{He} + {}^{209}\text{Bi}$ [28] and ${}^8\text{B} + {}^{58}\text{Ni}$ [29].

Fortunately, the total reaction cross section can be obtained from optical model analyses of experimental angular distributions of the elastic scattering. Therefore, comparison of the total reaction cross section data for different systems may bring some insights about the influence of nuclear structure or projectile configuration in the reaction mechanisms. However, to perform a systematic comparative studies of total reaction cross sections it is necessary to remove the contribution from the trivial properties of the colliding partners such as masses, charges and sizes. This can be achieved by reducing the total reaction cross sections according to some procedure. A reduction method was proposed by Canto *et al.*, which is based on Wong's analytic expression for fusion cross section, see Refs. [30–32].

The Wong's equation is derived considering barrier penetration at energies near and below the Coulomb barrier and it has been applied to fusion excitation function. The potential barrier is fitted by a parabola with maximum V_B located at R_B , and with a curvature parameter $\hbar\omega$. In this approximation the l -dependence of the effective potential is assumed to have the same radius and curvature parameter. This reduction method has been extended and applied to the total reaction cross section as well [33]. As discussed in Ref. [33], all the proposed reduction methods have some limitation, and, in principle, they would not work well for total reaction cross sections for systems with very different mass range of the colliding partners. However, if we apply this reduction method for a restricted number of systems with projectiles of similar mass and on the same target, we may be able to extract some general properties.

In this qualitative procedure, the Wong's equation for fusion is given by:

$$\sigma_F(E) = \frac{\hbar\omega}{2E} R_B^2 \times \ln \left[1 + \exp \left(2\pi \frac{E - V_B}{\hbar\omega} \right) \right]. \quad (1)$$

Based on this equation the energies and total reaction cross sections were transformed according to the following equations:

$$E_{c.m.} \rightarrow x = \frac{E_{c.m.} - V_B}{\hbar\omega} \quad (2)$$

and

$$\sigma_R(E) \rightarrow F(x) = \frac{2E}{\hbar\omega R_B^2} \times \sigma_R(E) \quad (3)$$

where σ_F has been replaced by σ_R .

When the reduction method is applied to the Wong cross section itself, one gets:

$$F_0(x) = \ln[1 + \exp(2\pi x)] \quad (4)$$

The $F_0(x)$ should represent the fusion contribution of the collision partners and can be used as benchmark, as stated in Refs. [30,31]. The F_0 is also called *universal fusion function* (UFF). The UFF is valid to describe fusion cross sections under the approximations used in the Wong's formula. Wong's formula may fail to describe fusion at the deep sub-barrier energies, but at near barrier energies, deviations can be interpreted as due to channel coupling effects.

Here we have applied this reduction method to the total reaction cross sections for several light projectiles on the ${}^{58}\text{Ni}$ and ${}^{64}\text{Zn}$ targets. The data for the systems used in the present analysis have been extracted from EXFOR database [1] and are listed in Table 1 with their corresponding references: ${}^6\text{He}$ [19], ${}^6\text{Li}$ [21,34,35], ${}^7\text{Li}$ [35,36], ${}^8\text{Li}$ [20], ${}^7\text{Be}$ [21], ${}^9,{}^{10},{}^{11}\text{Be}$ [37], ${}^8\text{B}$ [21], ${}^{10}\text{B}$ [22], ${}^{11}\text{B}$ [23], ${}^{12}\text{B}$ [24,25], ${}^{10}\text{C}$ [26], ${}^{12}\text{C}$ [38] and ${}^{16}\text{O}$ [39]. The experimental total reaction cross sections were obtained from the original paper. For those indicated by asterisk in Table 1 the total reaction cross sections were obtained by optical model calculation considering Wood-Saxon potential and the searching option (Sfresco) of the Fresco code [40]. The reduced total reaction cross sections ($F(x)$) as a function of the reduced energy (x) plot for these systems is shown in Fig. 1. The parameters of the potential, V_B , R_B and $\hbar\omega$, used in the reduction, were obtained with the Akyüs-Winther Potential [41]. These parameters are listed in Table 1. A discussion on how this potential works in the one-dimensional WKB (Wentzel, Kramers, Brillouin) barrier tunneling model related to fusion and optical model can be found in Ref. [42].

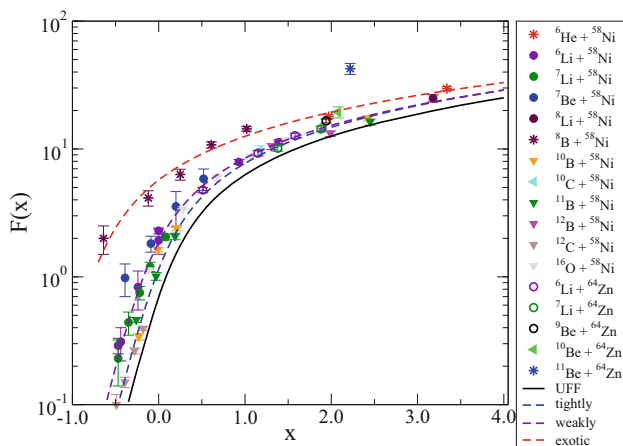
As we can observe in Fig. 1, the systems with exotic (${}^6\text{He}$, ${}^8\text{B}$ and ${}^{11}\text{Be}$) projectiles, with binding energies of less than 1.0 MeV, follow a different trend than those with tightly and weakly-bound projectiles. However, the difference in the trends for the tightly and weakly-bound projectiles is small. The solid curve in the Fig. 1 corresponds to the universal fusion function (UFF). To better identify the difference for the weakly and tightly-bound systems we performed a fitting procedure considering the data of some systems with a modified Wong's Equation given by:

$$\sigma(E) = p_1 \times \frac{\hbar\omega}{2E} R_B^2 \times \ln \left[1 + \exp \left(2\pi \left(\frac{E - V_B}{\hbar\omega} \right) - p_2 \right) \right] \quad (5)$$

This modified Wong's equation was applied to the tightly-bound (${}^{10}\text{B}$, ${}^{11}\text{B}$, ${}^{12}\text{C}$ and ${}^{16}\text{O}$), weakly-bound (${}^6\text{Li}$, ${}^7\text{Li}$, ${}^7\text{Be}$, ${}^9\text{Be}$) and exotic (${}^6\text{He}$ and ${}^8\text{B}$) projectiles reduced cross sections. The parameters p_1 and p_2 have no physical meaning and are introduced just to generate curves for exotic, weakly and tightly bound projectiles and guide the eyes for their different behaviors. These parameters were free to vary in the best fitting procedure. The results of the fittings are listed in Table 2 and the corresponding curves are indicated in Fig. 1

Table 1 Systems considered in the present analysis with the corresponding parameters of the Coulomb barrier, energies and references. For the systems indicated by asterisk symbol (*), the total reaction cross-sections were obtained in the present work

System	V_B (MeV)	R_B (fm)	$\hbar\omega$ (MeV)	energies E_{Lab} (MeV)	References
${}^6\text{He} + {}^{58}\text{Ni}$ (*)	8.2	9.17	3.43	16.5, 21.7	Morcelle-14 [19]
${}^6\text{Li} + {}^{58}\text{Ni}$	12.7	8.89	3.90	12.1, 13.0, 14.0	Aguilera-09 [21]
${}^6\text{Li} + {}^{58}\text{Ni}$ (*)	12.7	8.89	4.02	12.0, 14.0, 18.0, 20.0	Pfeifer-73 [34]
${}^7\text{Li} + {}^{58}\text{Ni}$	12.4	9.07	3.60	12.0, 12.5, 13.0, 13.5, 14.2	Valenzuela-17 [36]
${}^8\text{Li} + {}^{58}\text{Ni}$	12.2	9.24	3.38	26.1	Santos-19 [20]
${}^7\text{Be} + {}^{58}\text{Ni}$	16.9	8.87	4.20	17.1, 18.5, 19.9, 21.4	Aguilera-09 [21]
${}^8\text{B} + {}^{58}\text{Ni}$	21.1	8.88	4.57	20.7, 23.4, 25.3, 27.2, 29.3	Aguilera-09 [21]
${}^{10}\text{B} + {}^{58}\text{Ni}$ (*)	20.5	9.15	3.85	23.0, 24.0, 25.0, 35.0	Scarduelli-17 [22]
${}^{11}\text{B} + {}^{58}\text{Ni}$ (*)	20.2	9.39	3.73	23.0, 24.0, 25.0, 35.0	Deshmukh-15 [23]
${}^{12}\text{B} + {}^{58}\text{Ni}$	20.1	9.39	3.64	30.0, 33.0	Zevallos-19 [24,25]
${}^{10}\text{C} + {}^{58}\text{Ni}$ (*)	24.9	9.02	4.46	35.3	Guimaraes-19 [26]
${}^{12}\text{C} + {}^{58}\text{Ni}$ (*)	24.3	9.26	3.90	27.0, 27.5, 28.0, 28.5	Gasques-02 [38]
${}^{16}\text{O} + {}^{58}\text{Ni}$ (*)	31.8	9.44	3.96	40.0, 42.0, 44.0, 46.0, 48.0	West-75 [39]
${}^6\text{Li} + {}^{64}\text{Zn}$	13.4	9.04	4.24	17.0, 20.0, 22.0	Gomes-05 [35]
${}^7\text{Li} + {}^{64}\text{Zn}$	13.1	9.21	3.58	20.0, 22.0	Gomes-05 [35]
${}^9\text{Be} + {}^{64}\text{Zn}$	17.3	9.31	3.72	27.9	Di Pietro-10 [37]
${}^{10}\text{Be} + {}^{64}\text{Zn}$	17.1	9.45	3.56	28.3	Di Pietro-10 [37]
${}^{11}\text{Be} + {}^{64}\text{Zn}$	16.9	9.57	3.44	28.7	Di Pietro-10 [37]

**Fig. 1** Reduced cross section $F(x)$ as a function of reduced energy for the systems indicated. The black solid line corresponds to the benchmark curve of UFF while the dashed colored curves are for tightly, weakly and exotic system as described in the text

by the dashed blue, violet and red curves, respectively. As can be observed in the figure, the reduced cross sections are larger than the UFF curve for all systems. Considering that the UFF curve can be attributed to the fusion (absorption), the dashed curves indicate that direct reaction contributions are present for all the systems. For exotic nuclei (${}^6\text{He}$ and ${}^8\text{B}$), the reduced cross section is much higher indicating a strong contribution from direct reaction (breakup and trans-

Table 2 Parameters for the modified Wong's equation

Projectiles	P_1	P_2	χ_{red}^2
${}^6\text{He}, {}^8\text{B}$	1.09 (4)	5.25 (42)	4.54
${}^6\text{Li}, {}^7\text{Li}, {}^7\text{Be}, {}^9\text{Be}$	1.19 (3)	5.05 (4)	19.1
${}^{10}\text{B}, {}^{11}\text{B}, {}^{12}\text{C}, {}^{16}\text{O}$	1.09 (2)	1.50 (7)	2.23

fer). The small difference, in terms of trends, for the weakly and tightly-bound nuclei, prevents us to draw any strong conclusion about direct reaction contribution. We also have to consider that the inelastic excitation (target and projectile) can also contribute to the total reaction cross section.

In particular, the reduced total reaction cross sections for the ${}^{10}\text{Be} + {}^{64}\text{Zn}$ and ${}^{11}\text{Be} + {}^{64}\text{Zn}$ systems are found to be quite high. The total reaction cross section for ${}^{11}\text{Be}$ is twice that for the ${}^{10}\text{Be}$ [37]. The strong elastic scattering absorption, and consequently, the higher total reaction cross sections, for the ${}^{11}\text{Be}$ is attributed to its halo configuration and weak binding energy of neutron valence particle. The combination of these two effects induces a high breakup probability. The coupling of the breakup channel with the elastic scattering has been investigated by the continuum coupled channel calculation (CDCC), which actually reproduced the elastic scattering angular distribution [37]. In a recent paper, Di Pietro et al., found that the ${}^{10}\text{Be}$ core-excitation might be not so important

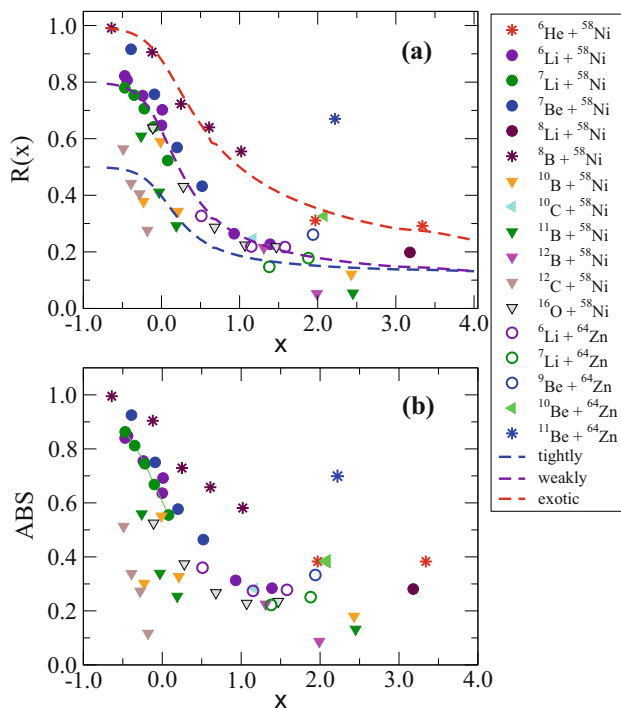


Fig. 2 Ratio cross section. **a** Difference between the reduced cross sections and F_0 . The colored dashed curves correspond to the calculated ratio for exotic, weakly and tightly-bound nuclei. **b** Difference between the reduced total reaction and absorption cross sections

as a coupling channel to describe the ${}^{11}\text{Be}$ elastic scattering but it is quite important to describe the breakup angular distribution [43]. The strong core-excitation is due to the large deformation of the ${}^{10}\text{Be}$, which might also be responsible for the enhancement of the total reaction cross section for this nucleus. Although ${}^{10}\text{Be}$ is a well bound nucleus, its reduced cross section lies very close to the red dashed curve designated for the exotic nuclei, most probably due to the strong absorption of the elastic flux by its large deformation.

The influence of direct reactions in the total reaction cross section can be better investigate by removing the fusion contribution from the experimental $F(x)$ values. This, actually, can be done in two ways: (1) by assuming that the UFF represents the contribution of the fusion reaction and removing it from the reduced total reaction cross section; (2) by considering the absorption cross section, calculated by a short range imaginary potential, and remove its contribution from the reduced total reaction cross section.

By considering that the UFF would represent the fusion cross section we can remove its contribution from the $F(x)$ and obtain the ratio:

$$R(x) = \frac{F(x) - F_0(x)}{F(x)} \quad (6)$$

This procedure has been already applied by Pakou et al., in Ref. [44]. In the present work we extend this procedure

to several other systems. The values of $R(x)$ for the systems listed in Table 1, as a function of the reduced energy are shown in Fig. 2a. The large difference between the different groups, tightly, weakly-bound and exotic projectiles can be now observed. This plot gives an indication of the contribution of direct reactions in the total reaction cross section. Therefore, it is clear that for exotic nuclei, direct reactions (breakup and transfer) are strong processes enhancing by quite a lot the total reaction cross section, in particular for energies very close and below the Coulomb barrier ($x < 0$). For the ${}^8\text{B}$ projectile, there is an indication that the direct channel would practically exhausts the total reaction cross sections for energies below the barrier [45], where the cross section for the breakup process, calculated by continuum discretization coupled channel (CDCC) calculation, gives the same value as the obtained total reaction cross section. Actually, this large predominance of direct reaction channel below the barrier has been corroborated by a recent experiment for the ${}^8\text{B} + {}^{208}\text{Pb}$ system, where the breakup was measured at a deep sub-barrier energy [46]. The predominance of direct reactions at energies below barrier has been also observed for the ${}^6\text{He} + {}^{209}\text{Bi}$ system [47]. It would be interesting to see whether this effect holds also for the neutron-rich nucleus ${}^{11}\text{Be}$ ($S_n = 0.501$ MeV). The $R(x)$ value for this nucleus is quite large even for energies above the Coulomb barrier. New measurements at different energies would be very welcome. It is important to mention that the effects of direct reaction channels on $R(x)$ might be overestimated for $x < 0$ in Fig. 2a as soon as the total fusion (TF) might be enhanced by these direct reaction channels at this energy regime. At energies above the barrier the effect of direct reaction channels on TF is usually very small.

The dashed curves in Fig. 2a corresponds to ratios given by Eq. 6 but using the fitted modified Wong's equation for the tightly-bound (${}^{10}\text{B}$, ${}^{11}\text{B}$, ${}^{12}\text{C}$ and ${}^{16}\text{O}$), weakly-bound (${}^6\text{Li}$, ${}^7\text{Li}$, ${}^7\text{Be}$, ${}^9\text{Be}$) and exotic (${}^6\text{He}$ and ${}^8\text{B}$) projectiles reduced cross sections. It is clear in Fig. 2a that the contribution of direct reactions is higher for weakly-bound nuclei compared to those for tightly-bound nuclei, in particular at energies close and below the Coulomb barrier. Although this might seem obvious, some other parameters such as deformations and cluster configuration would play important roles in the direct processes. This seems to be the case for the ${}^{10}\text{Be}$ and ${}^{10}\text{C}$ projectiles, which have the $(\alpha + \alpha + n + n)$ and $(\alpha + \alpha + p + p)$ cluster configurations, respectively. As already mentioned, the reduced total reaction for ${}^{10}\text{Be}$ is quite high, very close to the red-dashed curve for exotic nuclei. ${}^{10}\text{C}$ nucleus is not as tightly bound as ${}^{10}\text{Be}$ but it neither can be considered weakly bound nucleus. Its reduced total reaction cross section, however, is similar to those for the weakly bound ${}^6\text{Li}$ nucleus at the same reduced energy. Strong absorption due to the cluster configuration has been observed for the ${}^{10}\text{C} + {}^{58}\text{Ni}$ system [26], and more recently

for the $^{10}\text{C} + ^{208}\text{Pb}$ system [48]. Forthcoming study of the deformation and cluster configuration on the elastic scattering induced by these projectiles would therefore be quite interesting. However, to consider a more realistic description of these projectiles 5-body calculations would be required, which is still a challenge for the theoreticians.

The second option to remove the contribution of fusion reaction from the reduced total reaction cross sections is by considering the absorption cross section. The absorption cross section can be obtained by considering a short range imaginary potential in the optical model analysis. In the present work we adopted a short-range potential with Woods-Saxon shape and with the parameters: $W = 50$ MeV, $r_w = 1.06$ fm, and $a_w = 0.2$ fm, where r_w is the reduced radius which should be multiplied by the mass term $(A_P^{1/3} + A_T^{1/3})$ to give the actual radius of the potential, and a_w is the diffuseness parameter. A_P and A_T are the mass numbers of projectile and target, respectively. This potential has been discussed in Ref. [42] and also has been used in several other works where coupled channel calculations have been performed [22–24, 26, 48]. For the real part of the complex potential we adopted the Akyüs-Winther Potential [41].

To remove the contribution of the fusion from the total reaction cross section we have applied the same reduction for both total reaction and the absorption cross section and calculated the ratio R_{ABS} as:

$$R_{ABS}(x) = \frac{F(x) - F_{ABS}(x)}{F(x)} \quad (7)$$

Actually, the reduced absorption cross section, F_{ABS} , included also the contribution of the low-lying excited states of the ^{58}Ni and ^{64}Zn targets evaluated by coupled channel (CC) calculations. The states included in the level scheme of the couplings are listed in Table 3 and where obtained from NNDC databases [49]. In this case, the effect of the enhancement of the TF for $x < 0$ due to the coupling to the inelastic scattering of the targets is considered in the CC calculations. This ratio for the same systems listed in Table 1, as a function of x , is plotted and shown in Fig. 2b. The conclusions are more or less the same as those drawn for the results of Fig. 2a. The group of exotic nuclei (^6He and ^8B) have higher ratio, meaning a much stronger influence of direct reactions, followed by weakly-bound nuclei (^6Li , ^7Li , ^7Be and ^9Be) and then the tightly bound- nuclei (^{10}B , ^{11}B , ^{12}C and ^{16}O). One important difference between the results from removing UFF and absorption cross section is related to the $^{16}\text{O} + ^{58}\text{Ni}$ system. In Fig. 2a the cross section ratios for this system are together with those for the group of weakly-bound projectile, while in Fig. 2b, they are closer to those for tightly bound projectiles. This might be an indication on the importance of the inelastic channel, which is taken into account in the absorption cross section. In Fig. 2b also, the ratio for ^{11}Be is exceptionally large, while for ^{10}Be is about the same as the

Table 3 Spin-parity and energy of the states in ^{58}Ni and ^{64}Zn , from the NNDC database [49], considered in the coupled-channel calculations

^{58}Ni		^{64}Zn	
J^π	E (MeV)	J^π	E (MeV)
0^+	g.s.	0^+	g.s.
2^+	1.454	2^+	0.992
4^+	2.459	2^+	1.799
2^+	2.775	0^+	1.910
0^+	2.942	4^+	2.307
3^-	4.475		

exotic nuclei group. The ratio for ^8Li is found to be also large, probably due to the strong coupling of the neutron stripping reaction with the elastic channel. The influence of the single neutron transfer was investigated in the $^8\text{Li} + ^{90}\text{Zr}$ system and it is reported to be quite important to describe the elastic scattering [44].

3 Distance of interaction

Another phenomenological approach which can be used to investigate static and dynamic effects in the elastic scattering of light nuclei is based on the analysis of distances. Distances and radii play important roles in the analysis of elastic scattering data. For instance, potentials parameters in optical model analysis are more sensitive at the strong-absorption radii. To analyze the elastic scattering in terms of distances we plot the ratio of the elastic cross section to the Rutherford value, $d\sigma/d\sigma_{\text{Ruth}}$, as a function of the reduced distance of closest approach d on a Rutherford trajectory. We are, thus, assuming that the systems follow Rutherford trajectories, and thus, the distance of closest approach can still be used for a general discussion in terms of systematic behavior for elastic scattering at energies near and above the Coulomb barrier. In this work we are performing such systematic phenomenological analysis for several systems involving light projectile on ^{58}Ni and ^{64}Zn targets, and analyze their behavior in terms of distances.

The distance of closest approach depends on the incident energy and scattering angle in the center of mass (c.m.) frame as:

$$D = \frac{1}{2} \times \frac{Z_P Z_T e^2}{E_{c.m.}} \times \left(1 + \frac{1}{\sin(\theta_{c.m.}/2)} \right), \quad (8)$$

In its turn, the reduced distance of closest approach is given by:

$$d = D / (A_P^{1/3} + A_T^{1/3}) \quad (9)$$

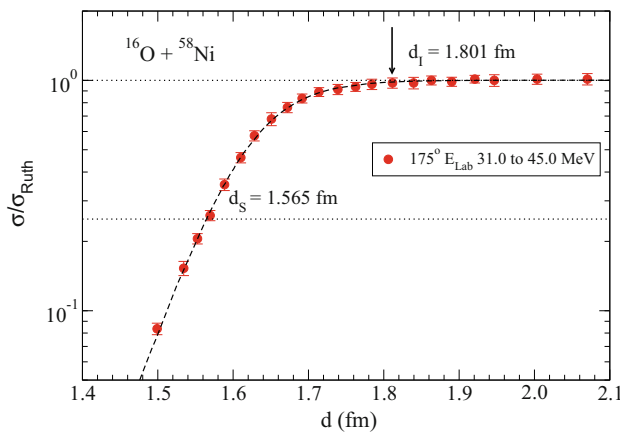


Fig. 3 Ratio of the elastic cross section to the Rutherford value, $d\sigma/d\sigma_{\text{Ruth}}$, as a function of the reduced distance of closest approach d for the $^{16}\text{O} + ^{58}\text{Ni}$ system [56]

where $[Z_P, A_P]([Z_T, A_T])$ correspond to the atomic and mass numbers of the projectile (target), respectively.

A sample of the plot $d\sigma/d\sigma_{\text{Ruth}}$ as a function of the reduced distance of closest approach d is shown in Fig. 3 for the $^{16}\text{O} + ^{58}\text{Ni}$ system. In this plot the elastic cross sections were measured at 175° (back-scattering) from $E_{\text{Lab}} = 31.0$ to 45.0 MeV. The ^{16}O projectile and the ^{58}Ni target can be considered strongly-bound nuclei with no static deformation. In this case, the $d\sigma/d\sigma_{\text{Ruth}}$ ratio is close to unity for larger distances and starts to fall off rapidly at short distances, due to strong absorption of the elastic flux into non-elastic channels (mostly fusion for this system).

From such plot we can extract the critical interaction distance, d_I , which is the distance where the interaction between the two colliding nuclei begins to be felt and the cross-section ratio starts deviating from unity. In this work we adopt a definition of the critical distance as the point where the ratio of elastic scattering to the Rutherford value is 0.98 or, in other words, when the absolute value of the S-matrix is 0.99. This is the distance where the flux from elastic scattering starts being absorbed. Another distance which can be obtained from this plot is the strong-absorption distance, d_S , where the ratio of elastic scattering to Rutherford drops to 0.25. Actually, the angle at which $d\sigma/d\sigma_R = 0.25$ ($\theta_{1/4}$) is called the “grazing angle”, and it corresponds to the distance where the elastic scattering is most sensitive to the optical-model potential.

Plots of $d\sigma/d\sigma_{\text{Ruth}}$ versus the reduced distance of closest approach, d , can be obtained from the direct conversion of the angular distributions ($d\sigma/d\sigma_{\text{Ruth}}$ as a function of angle) for a given energy. In this way we can combine several angular distributions in one plot. This is of particular importance for data involving radioactive ion beam projectiles since the cross sections are measured at few angles for each energy.

To more precisely and reliably determine the reduced distances we are adopting the same procedure as from Ref.

[50], where a Boltzmann exponential function, with three free parameters, is used to fit the cross section data.

$$y = \frac{p_1}{1 + e^{-p_2(d-p_3)}} \quad (10)$$

where $y = d\sigma/d\sigma_{\text{Ruth}}$, d is the reduced distance of closest approach, and p_1, p_2, p_3 are adjustable parameters, used to fit the data.

We should emphasize that this expression has no real physical meaning and it just has been used to provide a good fit to the data and to enable us to extract the distances of interest in a consistent way. Therefore, it is valid only for the limited range of distances of interest. Also, this expression is not useful to fit data with strong Fresnel peak in their elastic scattering angular distributions, as the case for $^{9,10}\text{Be} + ^{64}\text{Zn}$ [37] and $^{10,11}\text{B} + ^{58}\text{Ni}$ [22,23] systems and any of the other systems at energies much above the Coulomb barrier.

All parameters in Eq. 10 were free to vary during the fitting procedure. The parameter p_1 in Eq. 10 is associated to the asymptotic value of y for large distance d . This parameter is then intrinsically related to the normalization of the data, which should be close to the unity for large values of d . Pakou et al. [51] and, more recently, by Guimarães et al. [50], used this method to determine the critical interaction distances and strong interaction distances in collisions of different projectiles on ^{208}Pb .

The obtained parameters and the corresponding χ^2_{red} from the fits are listed in Table 4. The small reduced χ^2_{red} obtained for some system, such as ^8B and ^{10}C are due to the large error bars, while the large χ^2_{red} obtained for the $^{12}\text{C} + ^{58}\text{Ni}$ system is due to the very small uncertainties in the cross sections.

The result of the fitting applied to the spherical $^{16}\text{O} + ^{58}\text{Ni}$ system is shown in Fig. 3. The data from the literature were converted from $d\sigma/d\sigma_{\text{Ruth}}$ measured at 175° (back-scattering) as a function of energy to the $d\sigma/d\sigma_{\text{Ruth}}$ as a function of the distance of closest approach, without any additional normalization. The energies considered for this system were not so far from the Coulomb barrier. At these backward angles, the influence of the Fresnel peak is not expected to be important and the critical interaction distance can therefore be reliably determined. Both critical interaction distance and strong absorption distance were then obtained.

The reduced critical interaction distance obtained for $^{16}\text{O} + ^{58}\text{Ni}$ is $d_I = 1.80 \pm 0.01$ fm, which corresponds to a distance $D_I = 11.50 \pm 0.10$ fm. The reduced strong-absorption distance is found to be $d_S = 1.565 \pm 0.002$ for this system, corresponding to $D_S = 10.00 \pm 0.01$ fm, which is a little further from the classical grazing distance $R = 1.3 \times (A_P^{1/3} + A_T^{1/3}) = 8.30$ fm for this system. The uncertainties in d_I and d_S were taken to be one-half of the difference between distance where the ratios are 0.97 and 0.99, and, 0.24 and 0.26, respectively. It is important to mention that the final uncertainties reflects the data quality in terms of

Table 4 The reduced critical interaction distance, d_I , and the reduced strong-absorption distance, d_S (at which $d\sigma/d\sigma_{Ruth}$ is 0.98 and 0.25, respectively), for the systems indicated

System	Configuration	B.E. (MeV)	d_I (fm)	d_S (fm)	p_1	p_2	p_3	χ^2_{red}	References
${}^6\text{He}+{}^{58}\text{Ni}$	${}^4\text{He}+2n$	0.973	2.93 (13)	1.522 (15)	1.005 (12)	− 3.38 (15)	1.849 (28)	1.12	Morcelle-14 [19]
${}^6\text{Li}+{}^{58}\text{Ni}$	${}^4\text{He}+d$	1.474	2.22(6)	1.600(7)	1.002 (4)	− 7.99 (36)	1.745 (4)	0.23	Aguilera-09 [21]
${}^7\text{Li}+{}^{58}\text{Ni}$	${}^4\text{He}+t$	2.467	2.19(5)	1.582(7)	1.006 (3)	− 7.74 (13)	1.725 (16)	1.28	Valenzuela-17 [36]
${}^8\text{Li}+{}^{58}\text{Ni}$	${}^7\text{Li}+n$	2.032	2.23(3)	1.433 (10)	1.055 (50)	− 4.68 (29)	1.682 (28)	0.32	Santos-19 [20]
${}^7\text{Be}+{}^{58}\text{Ni}$	${}^4\text{He}+{}^3\text{He}$	1.587	2.17(6)	1.603(6)	1.001 (20)	− 8.81 (54)	1.728 (8)	0.26	Aguilera-09 [21]
${}^8\text{B}+{}^{58}\text{Ni}$	${}^7\text{Be}+p$	0.138	2.50 (10)	1.625 (10)	0.999 (4)	− 5.78 (27)	1.814 (10)	0.22	Aguilera-09 [21]
${}^{10}\text{B}+{}^{58}\text{Ni}$	${}^6\text{Li}+\alpha$	4.461	1.92(3)	1.574 (10)	1.008 (3)	− 13.28 (24)	1.657 (11)	1.76	Scarduelli-17 [22]
${}^{11}\text{B}+{}^{58}\text{Ni}$	${}^{10}\text{B}+n$	8.664	1.88(3)	1.587 (4)	1.007 (2)	− 16.16 (20)	1.656 (8)	2.41	Deshmukh-15 [23]
${}^{12}\text{B}+{}^{58}\text{Ni}$	${}^{11}\text{B}+n$	3.370	1.90(3)	1.556 (4)	1.029 (7)	− 13.18 (80)	1.637 (5)	2.66	Zevallos-19 [24]
${}^{10}\text{C}+{}^{58}\text{Ni}$	$\alpha + \alpha + p + p$	3.729	2.56 (16)	1.412 (12)	0.997 (10)	− 4.53 (60)	1.652 (30)	0.53	Guimaraes-19 [26]
${}^{12}\text{C}+{}^{58}\text{Ni}$	$\alpha + \alpha + \alpha$	7.275	1.83 (3)	1.570 (3)	1.004 (1)	− 18.31 (17)	1.629 (7)	15.0	Gasques-02 [38]
${}^{16}\text{O}+{}^{58}\text{Ni}$	${}^{12}\text{C}+\alpha$	7.162	1.80 (2)	1.572 (2)	1.007 (4)	− 20.97 (38)	1.624 (10)	3.50	Christensen-73 [56]
${}^4\text{He}+{}^{64}\text{Zn}$	${}^4\text{He}$		2.28 (5)	1.423 (11)	1.027 (4)	− 4.89 (5)	1.655(4)	1.93	Ornelas-04 [52]
${}^6\text{He}+{}^{64}\text{Zn}$	${}^4\text{He}+2n$	0.973	2.60 (12)	1.598 (12)	1.019 (17)	− 4.35 (18)	1.856 (18)	0.41	DiPietro-04 [53]
${}^6\text{Li}+{}^{64}\text{Zn}$	${}^4\text{He}+d$	1.474	2.27 (5)	1.592 (8)	1.005 (1)	− 7.06 (3)	1.747 (10)	3.25	Zadro-09 [54]
${}^9\text{Be}+{}^{64}\text{Zn}$	$\alpha + \alpha + n$	1.574	2.11 (5)	1.596(7)	1.012 (20)	− 8.82 (4)	1.721 (1)	7.3	DiPietro-10 [37] andMoraes-00 [55]
${}^{11}\text{Be}+{}^{64}\text{Zn}$	${}^{10}\text{Be}+n$	0.502	2.71 (13)	1.756 (10)	0.997 (2)	− 5.31 (19)	1.961 (8)	19.0	DiPietro-10 [37]

distribution of the data and the uncertainties in the individual cross sections. The difference between the reduced critical interaction and strong-absorption distances, $\Delta d = d_I - d_S$, which is 0.23 fm for ${}^{16}\text{O}$, corresponds to a region of the predominance for direct processes (inelastic excitation, breakup, transfer etc.) as the main source of absorption of the elastic flux.

The aim of the present work is to compare the reduced critical interaction and strong-absorption distances for different projectile types (exotic, weakly- and strongly-bound, stable and radioactive light nuclei) on the medium mass targets ${}^{58}\text{Ni}$ and ${}^{64}\text{Zn}$ and see if there is any correlation between these distances and, for instance, the binding energies of the projectile. The systems used in the present analysis are listed in Table 4, where the main configuration and the corresponding binding energy are also listed. In the present analysis we are including data on elastic scattering induced by tightly-bound (${}^{11}\text{B}$, ${}^{12}\text{C}$ and ${}^{16}\text{O}$), weakly-bound (${}^6\text{Li}$, ${}^7\text{Li}$, ${}^7\text{Be}$, ${}^8\text{Li}$ and ${}^9\text{Be}$) and exotic (${}^6\text{He}$, ${}^8\text{B}$ and ${}^{11}\text{Be}$) nuclei. The ${}^{10}\text{B}$, ${}^{12}\text{B}$ and ${}^{10}\text{C}$ nuclei, also considered in the present analysis, have binding energies lying between 2.5 and 4.0 MeV and can be classified as intermediate between tightly and weakly-bound nuclei.

The elastic scattering data for systems listed in Table 4 were extracted from the EXFOR database [1] but they are from: ${}^4\text{He}$ [52,53], ${}^6\text{He}$ [19,53], ${}^6\text{Li}$ [21,54], ${}^7\text{Li}$ [36], ${}^8\text{Li}$ [20], ${}^7\text{Be}$ [21], ${}^9\text{Be}$ [37,55], ${}^{11}\text{Be}$ [37], ${}^8\text{B}$ [21], ${}^{10}\text{B}$ [22], ${}^{11}\text{B}$

[23], ${}^{12}\text{B}$ [24], ${}^{10}\text{C}$ [26], ${}^{12}\text{C}$ [38] and ${}^{16}\text{O}$ [56]. The cross sections in the angular distribution as a function of angle were converted to distance and the fitting procedure, using Eq. 10 was applied. From the results of the fit the reduced critical interaction distance, d_I , and the reduced strong-absorption distance, d_S could be obtained and they are listed in Table 4, together with the values obtained for the parameter p_1 . As already mentioned the parameter p_1 is related to the asymptotic value for large distance and it should be close to one if the cross section ratio to the Rutherford, $d\sigma/d\sigma_{Ruth}$, is well normalized. The only data set which needed an extra normalization was the data for the ${}^6\text{He} + {}^{64}\text{Zn}$ system measured at $E_{Lab} = 28.7$ MeV by Di Pietro et al. [37].

In Figs. 4, 5 and 6 we show data for the projectile pairs ${}^6\text{Li}-{}^6\text{He}$, ${}^8\text{B}-{}^{11}\text{B}$ and ${}^{10}\text{C}-{}^{12}\text{C}$ on ${}^{58}\text{Ni}$ target and in Figs. 7 and 8 for the projectile pair ${}^{11}\text{Be}-{}^9\text{Be}$ and ${}^4\text{He}-{}^6\text{He}$ on ${}^{64}\text{Zn}$ target. The dashed curves in the figures are the results of the fits using Eq. 10, and the obtained distances of interaction and strong-absorption distance for each projectile are indicated.

Some conclusions can be drawn by inspecting the reduced distances indicated in the Figs. 4, 5, 6, 7 and 8 and listed in Table 4. The average reduced strong-absorption distances for exotic, weakly and tightly bound projectiles are $d_S = 1.58 \pm 0.15$ fm, 1.56 ± 0.07 fm and 1.57 ± 0.01 fm, respectively. Although they are about the same, within the error bars, the average strong-absorption distance, as well as the individual strong-absorption distance, is better evaluated for

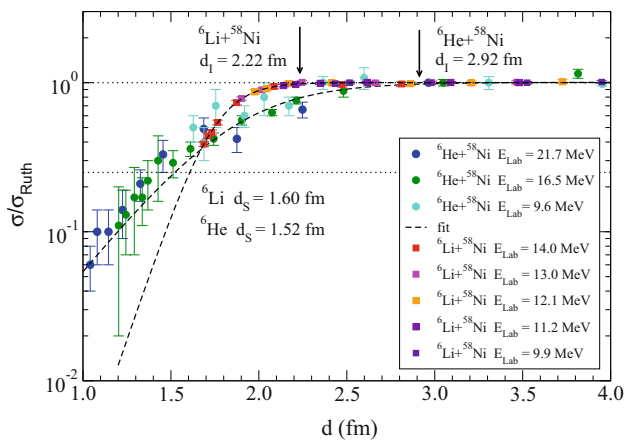


Fig. 4 Ratio of the elastic cross section to the Rutherford value, $d\sigma/d\sigma_{\text{Ruth}}$, as a function of the reduced distance of closest approach d for the ${}^6\text{Li} + {}^{58}\text{Ni}$ [21] and ${}^6\text{He} + {}^{58}\text{Ni}$ [19] systems

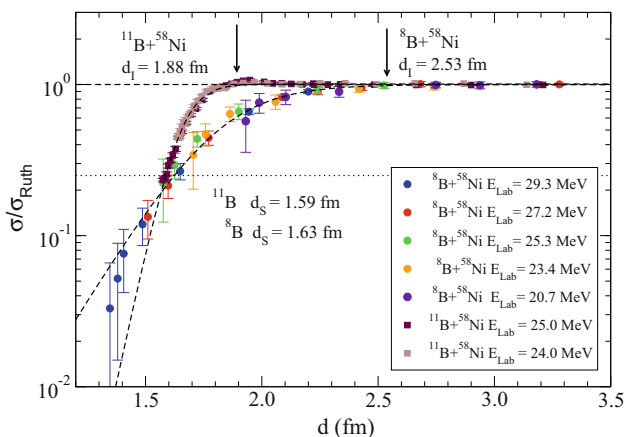


Fig. 5 Ratio of the elastic cross section to the Rutherford value, $d\sigma/d\sigma_{\text{Ruth}}$, as a function of the reduced distance of closest approach d for the ${}^8\text{B} + {}^{58}\text{Ni}$ [21] and ${}^{11}\text{B} + {}^{58}\text{Ni}$ [23] systems

the tightly bound nuclei, as can be observed from the standard deviation associated to each value. The largest deviation from the average value is obtained for the exotic ${}^{11}\text{Be}$ nucleus with $d_s = 1.76(1)$ fm and for ${}^{10}\text{C}$ with $d_s = 1.41(1)$ fm. About the reduced critical interaction distances, the average value for the systems with weakly-bound projectiles ${}^6\text{Li}$, ${}^7\text{Li}$, ${}^8\text{Li}$, ${}^7\text{Be}$ and ${}^9\text{Be}$ is $d_l = 2.18(49)$ fm, while for the tightly-bound system the average value is $d_l = 1.87(1)$ fm, where the uncertainty associated to each value is actually the standard deviation. For the exotic projectiles, ${}^6\text{He}$, ${}^8\text{B}$ and ${}^{11}\text{Be}$, the reduced critical distances are much larger and are in the range of $d_l = 2.5$ to 3.0 fm. The larger values observed for these exotic nuclei are primarily associated with the peripheral nature of their breakup process. Due to the extended matter density (static effect) (associated with lower breakup threshold, and stronger couplings to the continuum), the effect of nuclear forces is felt beyond the classical range of these forces, hence resulting in an early deviation of the

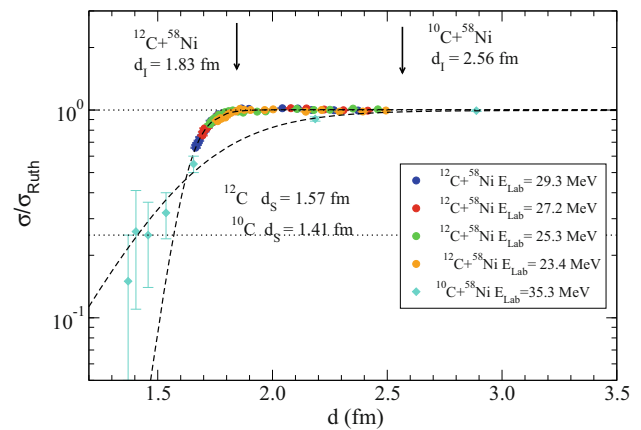


Fig. 6 Ratio of the elastic cross section to the Rutherford value, $d\sigma/d\sigma_{\text{Ruth}}$, as a function of the reduced distance of closest approach d for the ${}^{10}\text{C} + {}^{58}\text{Ni}$ [26] and ${}^{12}\text{C} + {}^{58}\text{Ni}$ [38] systems

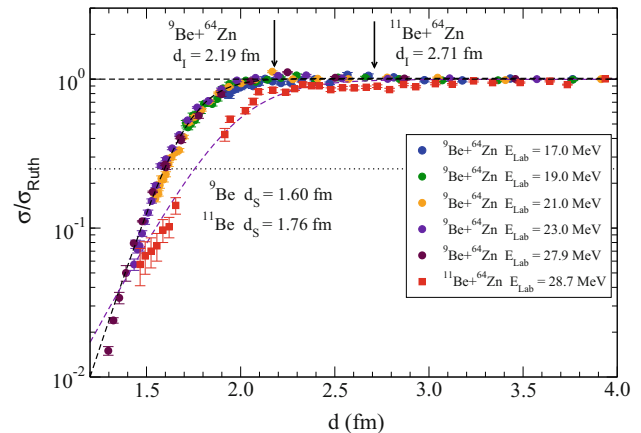


Fig. 7 Ratio of the elastic cross section to the Rutherford value, $d\sigma/d\sigma_{\text{Ruth}}$, as a function of the reduced distance of closest approach d for the ${}^9\text{Be} + {}^{64}\text{Zn}$ [55] and ${}^{11}\text{Be} + {}^{64}\text{Zn}$ [37] systems

$d\sigma/d\sigma_{\text{Ruth}}$ ratio from unity, owing to nuclear absorption at relatively large distance. An interesting effect, observed in Figs. 4, 5 and 6, is that for distances smaller than the reduced strong absorption distance, the absorption is stronger for the more bound projectiles. The small Fresnel peak observed in the angular distributions for the ${}^4\text{He} + {}^{64}\text{Zn}$ preventing us to reliably determine the reduced critical interaction distance. The obtained distance of $d_l = 2.28(5)$ seems to be too large. It is clear, however, that the distance is larger for the ${}^6\text{He}$ as compared to ${}^4\text{He}$. Also, as can be observed in Fig. 8, the reduced strong absorption distance is much smaller for ${}^4\text{He}$, indicating that this projectile reaches an inner region in the collision. For distances shorter than the reduced absorption distance, the absorption is weaker for ${}^4\text{He}$ in opposite to what is observed for the other tightly bound systems investigated in the present work.

The above discussed effects can be clearly observed in Fig. 9 where the reduced critical distance of interaction is

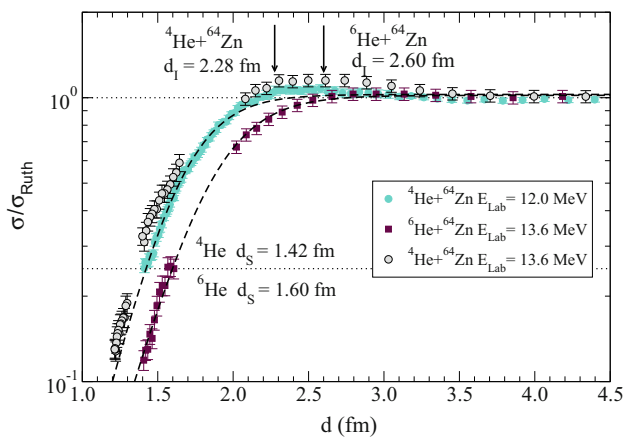


Fig. 8 Ratio of the elastic cross section to the Rutherford value, $d\sigma/d\sigma_{\text{Ruth}}$, as a function of the reduced distance of closest approach d for the $^4\text{He} + ^{64}\text{Zn}$ at $E_{\text{Lab}} = 13.6$ MeV [53] and $^4\text{He} + ^{64}\text{Zn}$ at $E_{\text{Lab}} = 10.0$ MeV [52] systems

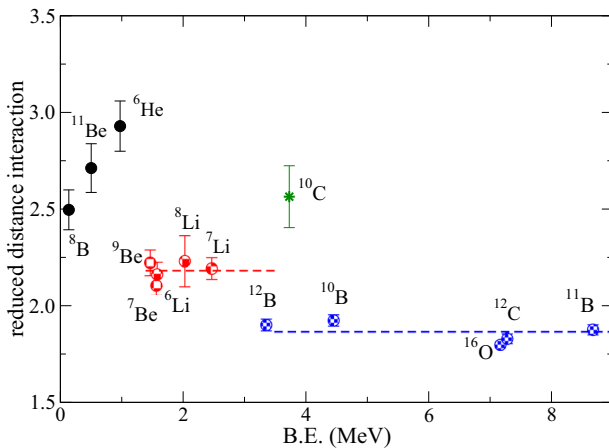


Fig. 9 Reduced critical distance of interaction as a function of the binding energy for the nuclei indicated. The dashed curve indicates the trend of the data for the weakly (red) and tightly bound nuclei (blue)

plotted as a function of the binding energy, for the systems on ^{58}Ni target. Inspecting closely Table 4, and Fig. 9, it follows that for exotic systems, lower breakup threshold alone cannot explain larger d_I values. One sees that although ^8B has the lowest breakup threshold, it corresponds to a smaller d_I , compared to ^6He and ^{11}Be . Notice that for the latter two systems, there is neither Coulomb nor centrifugal barriers which the valence neutron(s) needs to tunnel through, which are both present for ^8B . One of the effects of this barrier is to confine the valence proton closer to the core nucleus, thus reducing the extension at larger distance of the matter density, which reduces the effect of the nuclear forces beyond the projectile-target distance. Therefore, these results further serve to highlight the importance of the ground-state configuration in the breakup process.

Also, the extended direct-interaction region for the ^6He and ^{11}Be projectiles corroborates the importance of the long-

range Coulomb and/or nuclear interaction for these exotic projectiles, as also observed in the reduction of the Fresnel diffraction peak in the corresponding angular distributions. The combination of the effect of the large value of the Coulomb dipole polarizability, as well as the large transfer/breakup probabilities observed experimentally, can also be the reason for the large value of the interaction distance for ^6He and ^{11}Be .

The critical interaction distance for ^{10}C stands out in the plot of Fig. 9. As already mentioned this nucleus has the exotic $\alpha - \alpha - p - p$ configuration and it is the only nucleus supposed to have a *brunnian* (*super-borromean*) structure [17]. As highlighted in the previous section, a large total reaction cross section has observed for this nucleus, even though it is quite bound. Although not completely clear, both large total reaction cross section and critical distance of interaction can be attributed to the strong absorption of elastic flux due to a combination of deformation and cluster configuration [26,48]. Further investigation about the role of deformation for ^{10}Be and ^{10}C projectile in the elastic scattering is on the way.

Since we are considering the reduced distances, the size and geometric effect of the projectiles, purely based on the mass dependence, should be washed out. The remaining size (geometric) effect would be then associated to deformation, cluster and halo configurations of the projectile. However, it is clear from the present analysis that the critical interaction distances are also influenced by the reaction mechanisms, which could be related to the binding energy. This is the case for the halo nuclei ^6He , ^8B and ^{11}Be , where the critical interaction distances should also depend on the binding energy of valence particles affecting the strength of the couplings for different incident energies. From the Fig. 8 we can see a correlation between the critical distance of interaction and the binding energy. This correlation is not as smooth as the one observed for the analysis on a heavier (^{208}Pb) target [50], but it is clearly present.

4 Summary

In the present work we performed a phenomenological analysis on the elastic scattering of light projectiles, tightly-bound (^{10}Be , ^{11}B , ^{12}C , ^{16}O), weakly-bound (^6Li , ^7Li , ^8Li , ^9Be), exotic (^6He , ^8B and ^{11}Be) plus ^{10}B , ^{10}C and ^{12}B nuclei on ^{58}Ni and ^{64}Zn targets at energies close to the Coulomb barrier. We considered the total reaction cross section, and distance of interaction, properly reduced, to infer about cluster configuration and dynamic effects. For the total reaction cross section, the important question is if the reduction can lead to a clear separation between tightly bound and stable or radioactive weakly bound systems. In the present work we

plot the reduced total reaction cross sections for several light projectiles and used the $F_0(x)$ (UFF) function as benchmark.

The influence of direct reaction is studied by removing the fusion contribution (UFF and absorption) from the total reaction cross section. Static and dynamic effects in the elastic scattering process at low energies could also be investigated using the semi-classical approach where the ratio of elastic cross sections to the Rutherford value were plotted as a function of the distance of closest approach on a Rutherford trajectory. From such plot the critical-interaction and strong-absorption distances were extracted from elastic data. The large values of the critical interaction distance for the exotic nuclei (^6H , ^8B and ^{11}Be) on medium mass targets (^{58}Ni and ^{64}Zn) corroborated the finding for the heavier ^{208}Pb target [50], where large values were also obtained for exotic projectile. For medium size target the mechanism seems to be the same, i.e., the combination of the effect of the large value of the Coulomb dipole polarizability, as well as the large transfer/breakup probabilities. Although not as clear as for the heavier ^{208}Pb target, a correlation between the critical interaction distance and the breakup threshold energy for a given cluster configuration was also observed for medium mass targets.

Acknowledgements The authors would like to thank São Paulo Research Foundation (FAPESP) (Grants 2016/17612-7, 2018/18241-8, 2019/07767-1), Conselho Nacional de Desenvolvimento Científico (CNPq) (Grant 304961/2017-5) and PNPd/CAPES 88887.475459/2020-00 for the financial support. The authors also thank INCT-FNA (Instituto Nacional de Ciência e Tecnologia- Física Nuclear e Aplicações, research project 464898/2014-5). E. F. A. would like to thank CONA-CyT for partial support (Grant no. CB-01-254619).

Data Availability Statement This manuscript has no associated data or the data will not be deposited. [Authors' comment: No new experimental data were presented in this paper. The data were obtained from the EXFOR data library or from the original published papers as indicated in Tables 1 and 4.]

References

1. N. Otuka, E. Dupont, V. Semkova, B. Pritychenko, A.I. Blokhin, M. Aikawa, S. Babykina, M. Bossant, G. Chen, S. Dunaeva, R.A. Forrest, T. Fukahori, N. Furutachi, S. Ganesan, Z. Ge, O.O. Gritzay, M. Herman, S. Hlavac, K. Kato, B. Lalremruata, Y.O. Lee, A. Makinaga, K. Matsumoto, M. Mikhaylyukova, G. Pikulina, V.G. Pronyaev, A. Saxena, O. Schwerer, S.P. Simakov, N. Soppera, R. Suzuki, S. Takacs, X. Tao, S. Taova, F. Tarkanyi, V.V. Varlamov, J. Wang, S.C. Yang, V. Zerkov, Y. Zhuang, Towards a more complete and accurate experimental nuclear reaction data library (EXFOR): international collaboration between nuclear reaction data centres (NRDC). *Nucl. Data Sheets* **120**, 272 (2014)
2. A. Karpov, A. Denikin, M. Naumenko, A. Alekseev, V. Rachkov, V. Samarin, V. Saiko, V. Zagrebaev, NRV web knowledge base on low-energy nuclear physics. *Nucl. Instrum. Methods Phys. Res. A* **859**, 112 (2017)
3. V.I. Zagrebaev, A.S. Denikin, A.V. Karpov, A.P. Alekseev, M.A. Naumenko, V.A. Rachkov, V.V. Samarin, V.V. Saiko, NRV web-knowledge base on low-energy nuclear physics (1999), <http://nrw.jinr.ru/>
4. M.S. Hussein, The unitarity defect of the S-matrix and the underlying absorptive potential II. The case of energy-dependent optical potentials. *Ann. Phys.* **177**, 58 (1987)
5. M.S. Hussein, The unitarity defect of the S-matrix and the underlying absorptive potential. *Ann. Phys.* **175**, 197 (1987)
6. L.F. Canto, R. Donangelo, M.S. Hussein, A. Lepine-Szily, Multi-step α -particle-transfer description of anomalous heavy-ion elastic scattering. *Phys. Rev. Lett.* **51**, 95 (1983)
7. M.S. Hussein, V.L.M. Franzin, R. Franzin, A.J. Baltz, Small effects in sub-barrier heavy-ion elastic scattering. *Phys. Rev. C* **30**, 184 (1984)
8. M.P. Pato, M.S. Hussein, Refraction-diffraction interference in heavy-ion elastic angular distributions. *Phys. Lett. B* **207**, 121 (1988)
9. M. Ueda, M.P. Pato, M.S. Hussein, Forward glory phenomenon in the dark-side of heavy-ion nuclear rainbow scattering. *Phys. Rev. Lett.* **81**, 1809 (1998)
10. J.J. Kolata, V. Guimarães, E.F. Aguilera, Elastic scattering, fusion, and breakup of light exotic nuclei. *Eur. Phys. J. A* **53**, 123 (2016)
11. L.F. Canto, V. Guimarães, J. Lubian, M.S. Hussein, The total reaction cross section of heavy-ion reactions induced by stable and unstable exotic beams: The low-energy regime. *Eur. J. Phys. A* **56**, 281 (2020)
12. L.F. Canto, P.R.S. Gomes, R. Donangelo, J. Lubian, M.S. Hussein, Recent developments in fusion and direct reactions with weakly bound nuclei. *Phys. Rep.* **596**, 1 (2015)
13. O.A. Rubtsova, V.I. Kukulin, A.M. Moro, Continuum discretization methods in a composite particle scattering off a nucleus: Benchmark calculations. *Phys. Rev. C* **78**, 034603 (2008)
14. P. Capel, F.M. Nunes, Benchmarking models of breakup reactions. *J. Phys. Conf. Ser.* **312**, 082015 (2011)
15. P. Descouvemont, M.S. Hussein, Towards a microscopic description of reactions involving exotic nuclei. *Phys. Rev. Lett.* **111**, 082701 (2013)
16. C. Liang, K. Mislav, On Borromean links. *J. Math. Chem.* **16**, 27 (1994)
17. N. Curtis, N.L. Achouri, N.I. Ashwood, H.G. Bohlen, W.N. Catford, N.M. Clarke, M. Freer, P.J. Haigh, B. Laurent, N.A. Orr, N.P. Patterson, N. Soic, J.S. Thomas, V. Ziman, Breakup reaction study of the Brunnian nucleus ^{10}C . *Phys. Rev. C* **77**, 021301(R) (2008)
18. I. Tanihata, H. Savajols, R. Kanungo, Recent experimental progress in nuclear halo structure studies. *Prog. Part. Nucl. Phys.* **68**, 215 (2013)
19. V. Morcelle, K.C.C. Pires, M. Rodriguez-Gallardo, R. Lichtenthaler, A. Lepine-Szily, V. Guimaraes, P.N. de Faria, D.R. Mendes Jr., A.M. Moro, L.R. Gasques, E. Leistenschneider, R.P. Condori, V. Scarduelli, M.C. Morais, A. Barioni, J.C. Zamora, J.M.B. Shorto, Four-body effects in the $^6\text{He}+^{58}\text{Ni}$ scattering. *Phys. Lett. B* **732**, 228 (2014)
20. O.C.B. Santos, R. Lichtenthaler Fo, K.C.C. Pires, A. Moro, U. Umbelino, E.O.N. Zevallos, M. Assuncao, S. Appannababu, A.L. Lara, V. Scarduelli, V. Guimarães, A. Lepine-Szily, A. Serra, R. Linares, V. Zagatto, M.C. Morais, A. Barioni, J.M.B. Shorto, Spin-orbit effects in the $^8\text{Li}+^{58}\text{Ni}$ elastic scattering. *J. Phys. Conf. Ser.* **1291**, 012030 (2019)
21. E.F. Aguilera, E. Martinez-Quiroz, D. Lizcano, A. Gomez-Camacho, J.J. Kolata, L.O. Lamm, V. Guimarães, R. Lichtenthaler, O. Camargo, F.D. Becchetti, H. Jiang, P.A. DeYoung, P.J. Mears, T.L. Belyaeva, Reaction cross sections for ^8B , ^7Be , and $^6\text{Li}+^{58}\text{Ni}$ near the Coulomb barrier: Proton-halo effects. *Phys. Rev. C* **79**, 021601(R) (2009)
22. V. Scarduelli, E. Crema, V. Guimarães, D. Abriola, A. Arazi, E. de Barbara, O.A. Capurro, M.A. Cardona, J. Gallardo, D. Hojman, G.V. Marti, A.J. Pacheco, D. Rodrigues, Y.Y. Yang, N.N.

- Deshmukh, B. Paes, J. Lubian, D.R. Mendes Jr., V. Morcelle, D.S. Monteiro, Elastic and inelastic scattering for the $^{10}\text{B}+^{58}\text{Ni}$ system at near-barrier energies. *Phys. Rev. C* **96**, 054610 (2017)
23. N.N. Deshmukh, V. Guimarães, E. Crema, D. Abriola, A. Arazi, E. de Barbara, O.A. Capurro, M.A. Cardona, J. Gallardo, D. Hojman, G.V. Marti, A.J. Pacheco, D. Rodrigues, Y.Y. Yang, A.N. Deshmukh, D.R. Mendes, V. Morcelle, V. Scarduelli, D.S. Monteiro, Elastic and inelastic scattering for the $^{11}\text{B}+^{58}\text{Ni}$ system: Target and projectile reorientation effects. *Phys. Rev. C* **92**, 054615 (2015)
 24. E.O.N. Zevallos, V. Guimarães, E.N. Cardozo, J. Lubian, R. Linares, R. Lichtenthaler Filho, K.C.C. Pires, O.C.B. Santos, S. Appannababu, E. Crema, J. Alcantara-Nunez, A.L. Lara, Y.S. Villamizar, U. Umbelino, N. Added, M. Assuncao, V. Morcelle, D.S. Monteiro, Elastic scattering of the $^{12}\text{B}+^{58}\text{Ni}$ system at near-barrier energies. *Phys. Rev. C* **99**, 064613 (2019)
 25. E.O.N. Zevallos, V. Guimarães, E.N. Cardozo, J. Lubian, O.C.B. Santos, R. Linares, M. Assuncao, J. Alcantara-Nunez, A.L. de Lara, R. Lichtenthaler Filho, K.C.C. Pires, U.U. da Silva, S. Appannababu, N. Added, D.S. Monteiro, V. Morcelle, Elastic scattering and total reaction cross section for the $^{12}\text{B}+^{58}\text{Ni}$ system. *J. Phys. Conf. Ser.* **1291**, 012029 (2019)
 26. V. Guimarães, E.N. Cardozo, V.B. Scarduelli, J. Lubian, J.J. Kolata, P.D. O'Malley, D.W. Bardayan, E.F. Aguilera, E. Martinez-Quiroz, D. Lizcano, A. Garcia-Flores, M. Febraro, C.C. Lawrence, J. Riggin, R.O. Torres-Isea, P.N. de Faria, D.S. Monteiro, E.S. Rossi, N.N. Deshmukh, Strong coupling effect in the elastic scattering of the $^{10}\text{C}+^{58}\text{Ni}$ system near barrier. *Phys. Rev. C* **100**, 034603 (2019)
 27. V. Guimarães, E.O.N. Zevallos, E.N. Cardozo, J. Lubian, O.C.B. Santos, R. Linares, M. Assuncao, J. Alcantara-Nunez, A.L. de Lara, R. Lichtenthaler, K.C.C. Pires, U.U. da Silva, S. Appannababu, Added, D.S. Monteiro, V. Morcelle, Cluster configuration effects in the elastic scattering of boron isotopes ^8B , ^{10}B , ^{11}B and ^{12}B on ^{58}Ni . *Recent Progress Few-Body Phys.* **238**, 195 (2020)
 28. E.F. Aguilera, J.J. Kolata, L. Acosta, Evidence for core-halo decoupling in halo systems. *Phys. Rev. C* **81**, 011604(R) (2010)
 29. J.J. Kolata, E.F. Aguilera, V. Guimarães, Near and sub-barrier reactions of ^8B . *EPJ Web Conf.* **163**, 00031 (2017)
 30. L.F. Canto, P.R.S. Gomes, J. Lubian, L.C. Chamon, E. Crema, Reduction of fusion and reaction cross sections at near-barrier energies. *J. Phys. G: Nucl. Part. Phys.* **36**, 015109 (2009)
 31. L.F. Canto, P.R.S. Gomes, J. Lubian, L.C. Chamon, E. Crema, Dynamic effects of breakup on fusion reactions of weakly bound nuclei. *Nucl. Phys. A* **821**, 51 (2009)
 32. L.F. Canto, D.R. Mendes Junior, P.R.S. Gomes, J. Lubian, Reduction of fusion and reaction cross sections at near-barrier energies. *Phys. Rev. C* **92**, 014626 (2015)
 33. J.M.B. Shorto, P.R.S. Gomes, J. Lubian, L.F. Canto, S. Mukherjee, L.C. Chamon, Reaction functions for weakly bound systems. *Phys. Lett. B* **678**, 77 (2009)
 34. K.O. Pfeiffer, E. Speth, K. Bethge, Break-up of ^6Li and ^7Li on Tin and Nickel Nuclei. *Nucl. Phys. A* **206**, 545 (1973)
 35. P.R.S. Gomes et al., Effect of the breakup on the fusion and elastic scattering of weakly bound projectiles on ^{64}Zn . *Phys. Rev. C* **71**, 034608 (2005)
 36. P. Amador-Valenzuela et al., Measurements of angular distributions for ^7Li elastically scattered from ^{58}Ni at energies around the Coulomb barrier. *J. Phys. Conf. Ser.* **876**, 012002 (2017)
 37. A. Di Pietro, G. Randisi, V. Scuderi, L. Acosta, F. Amorini, M.J.G. Borge, P. Figuera, M. Fischella, L.M. Fraile, J. Gomez-Camacho, H. Jeppesen, M. Lattuada, I. Martel, M. Milin, A. Musumarra, M. Papa, M.G. Pellegriti, F. Perez-Bernal, R. Raabe, F. Rizzo, D. Santonocito, G. Scalia, O. Tengblad, D. Torresi, A.M. Vidal, D. Voulot, F. Wenander, M. Zadro, Elastic scattering and reaction mechanisms of the halo nucleus ^{11}Be around the coulomb barrier. *Phys. Rev. Lett.* **105**, 022701 (2010)
 38. L.R. Gasques, L.C. Chamon, C.P. Silva, D. Pereira, M.A.G. Alvarez, E.S. Rossi Jr., V.P. Likhachev, B.V. Carlson, C. De Conti, Determination of the ^{12}C nuclear density through heavy-ion elastic scattering experiments. *Phys. Rev. C* **65**, 044314 (2002)
 39. L. West Jr., K.W. Kemper, N.R. Fletcher, Elastic scattering of ^{16}O by even mass nickel isotopes. *Phys. Rev. C* **11**, 859 (1975)
 40. I.J. Thompson, Coupled channels methods for nuclear physics. *Comput. Phys. Rep.* **7**, 167 (1988)
 41. O. Akyüz, A. Winther, in *Nuclear Structure of Heavy Ion Reaction*, edited by R. A. Broglia, C. H. Dasso, and R. A. Ricci (North Holland, 1981), *Proc. E. Fermi Summer School of Physics* (1981)
 42. L.F. Canto, R. Donangelo, M.S. Hussein, P. Lotti, J. Lubian, J. Rangel, Theoretical considerations about heavy-ion fusion in potential scattering. *Phys. Rev. C* **98**, 044617 (2018)
 43. A. Di Pietro, A.M. Moro, Jin Leib, R. de Diego, Insights into the dynamics of breakup of the halo nucleus ^{11}Be on a ^{64}Zn target. *Phys. Lett. B* **798**, 134954 (2019)
 44. A. Pakou, D. Pierrousakou, M. Mazzocco, L. Acosta, X. Aslanoglou, A. Boiano, C. Boiano, D. Carbone, M. Cavallaro, J. Grebosz, N. Keeley, M. La Commara, C. Manea, G. Marquez-Duran, I. Martel, C. Parascandolo, K. Rusek, A.M. Sanchez-Benitez, O. Sgouros, C. Signorini, F. Soramel, V. Soukeras, E. Stiliaris, E. Strano, D. Torresi, A. Trzcinska, Y.X. Watanabe, H. Yamaguchi, Total reaction cross sections for $^8\text{Li}+^{90}\text{Zr}$ at near-barrier energies. *Eur. Phys. J. A* **51**, 55 (2015)
 45. E.F. Aguilera, P. Amador-Valenzuela, E. Martinez-Quiroz, D. Lizcano, P. Rosales, H. Garcia-Martinez, A. Gomez-Camacho, J.J. Kolata, A. Roberts, L.O. Lamm, G. Rogachev, V. Guimaraes, F.D. Becchetti, A. Villano, M. Ojaruega, M. Febraro, Y. Chen, H. Jiang, P.A. DeYoung, G.F. Peaslee, C. Guess, U. Khadka, J. Brown, J.D. Hinnefeld, L. Acosta, E.S. Rossi Jr., J.F.P. Huiza, T.L. Belyaeva, Near-Barrier Fusion of the $^8\text{B}+^{58}\text{Ni}$ Proton-Halo System. *Phys. Rev. Lett.* **107**, 092701 (2011)
 46. A. Pakou, L. Acosta, P.D. O'Malley, S. Aguilar, E.F. Aguilera, M. Baines, D. Bardayan, F.D. Becchetti, Ch. Boomersshine, M. Brodeur, F. Cappuzzello, S. Carmichael, L. Caves, E. Chavez, C. Flores-Vazquez, A. Gula, J.J. Kolata, B. Liu, D.J. Marin-Lambarri, F.F. Morales, K. Rusek, A.M. Sanchez-Benitez, O. Sgouros, V.R. Sharma, V. Soukeras, G. Souliotis, Dominance of direct reaction channels at deep sub-barrier energies for weakly bound nuclei on heavy targets: The case $^8\text{B} + ^{208}\text{Pb}$. *Phys. Rev. C* **101**, 024602 (2020)
 47. J.J. Kolata, Transfer, breakup, and fusion reactions of ^6He with ^{209}Bi near the Coulomb barrier. *Eur. Phys. J. A* **13**, 117–121 (2002)
 48. R. Linares, E. N. Cardozo, M. Sinha, V. Guimarães, et al., under review to *Phys. Rev. C* (2020)
 49. B. Pritychenko, E. Betak, M.A. Kellett, S. Singh, J. Totans, The nuclear science references (NSR) database and web retrieval system. *Nucl. Inst. Method Phys. Res. Sect. A* **640**, 213 (2011)
 50. V. Guimarães, J. Lubian, J.J. Kolata, E.F. Aguilera, M. Assuncao, V. Morcelle, Phenomenological critical interaction distance from elastic scattering measurements on a ^{208}Pb target. *Eur. J. Phys. A* **52**, 223 (2018)
 51. A. Pakou, K. Rusek, Interaction distances for weakly bound nuclei at near barrier energies. *Phys. Rev. C* **69**, 057602 (2004)
 52. A. Ornelas, P. Mohr, Gy Gyurky, Z. Elekes, Zs Fulop, Z. Halasz, G.G. Kiss, E. Somorjai, T. Szucs, M.P. Takacs, D. Galaviz, R.T. Guray, Z. Korkulu, N. Ozkan, C. Yalcin, α scattering and α -induced reaction cross sections of ^{64}Zn at low energies. *Phys. Rev. C* **94**, 055807 (2016)
 53. A. Di Pietro, P. Figuera, F. Amorini, C. Angulo, G. Cardella, S. Cherubini, T. Davinson, D. Leanza, J. Lu, H. Mahmud, M. Milin, A. Musumarra, A. Ninane, M. Papa, M.G. Pellegriti, R. Raabe, F. Rizzo, C. Ruiz, A.C. Shotton, N. Soic, S. Tudisco, L. Weissman, Reactions induced by the halo nucleus ^6He at energies around the Coulomb barrier. *Phys. Rev. C* **69**, 044613 (2004)

54. M. Zadro, P. Figuera, A. Di Pietro, F. Amorini, M. Fisichella, O. Goryunov, M. Lattuada, C. Maiolino, A. Musumarra, V. Ostashko, M. Papa, M.G. Pellegriti, F. Rizzo, D. Santonocito, V. Scuderi, D. Torresi, Elastic scattering of ^6Li on ^{64}Zn at near-barrier energies. *Phys. Rev. C* **80**, 064610 (2009)
55. S.B. Moraes, P.R.S. Gomes, J. Lubian, J.J.S. Alves, R.M. Anjos, M.M. Sant'Anna, I. Padron, C. Muri, R. Liguori Neto, N. Added, Fusion and elastic scattering of $^9\text{Be}+^{64}\text{Zn}$: a search of the breakup influence on these processes. *Phys. Rev. C* **61**, 64608 (2000)
56. P.R. Christensen, I. Chernov, E.E. Gross, R. Stokstad, F. Videbaek, The interference of coulomb and nuclear excitation in the scattering of ^{16}O from ^{58}Ni , ^{88}Sr and ^{142}Nd . *Nucl. Phys. A* **207**, 433 (1973)